Ellagic acid inhibits tumor growth and potentiates the therapeutic efficacy of sorafenib in hepatocellular carcinoma

Zhenju Tan [a],[1], Xuemei Li [b],[1], Xia Chen [b],[1], Li Wang [b], Baijun Chen [b], Sichong Ren [c],[**], Ming Zhao [b],[*]

[a] Department of Gastroenterology, The Affiliated Hospital of Southwest Medical University, Luzhou, 646000, PR China
[b] Department of Gastroenterology, Clinical Medical College and the First Affiliated Hospital of Chengdu Medical College, Chengdu, 610500, PR China
[c] Department of Nephrology, Clinical Medical College and the First Affiliated Hospital of Chengdu Medical College, Chengdu, 610500, PR China

ARTICLE INFO

ABSTRACT

Background: Sorafenib is a classic molecular targeted drug approved for hepatocellular carcinoma (HCC) therapy. However, a poor response rate and increasing resistance to sorafenib make its therapeutic efficacy suboptimal. Combination treatment with an agent capable of potentiating sorafenib sensitivity may be a promising solution.
Aim: The aim of this study was to determine the synergistic effect of ellagic acid (EA), a natural polyphenol, and sorafenib on HCC.
Methods: CCK-8, EdU incorporation and colony formation assays were used to study the effect of EA on HCC cell proliferation. Apoptosis was detected by flow cytometry in HCC cells and TUNEL assay in xenograft tumors. Transcriptome analysis was utilized to investigate alterations in signaling pathways with EA treatment. A xenograft mouse model was used to confirm the synergistic effect of sorafenib and EA on HCC tumors *in vivo*.
Results: We found that EA inhibited growth and induced apoptosis in both HCC cells and xenograft tumors. Mechanistically, EA treatment reduced the activation of the MAPK and Akt/mTOR signaling pathways in HCC cells. Furthermore, combined EA and sorafenib treatment further inhibited the MAPK and Akt/mTOR signaling pathways compared to EA or sorafenib alone. EA synergistically potentiated the anticancer activity of sorafenib against HCC both *in vitro* and *in vivo*.
Conclusion: EA inhibits HCC growth by inducing apoptosis through attenuation of the MAPK and Akt/mTOR signaling pathways. EA potentiates the response of HCC tumors to sorafenib both *in vitro* and *in vivo*, an effect that may be attributed to further inhibition of the MAPK and Akt/mTOR signaling pathways. These results suggest that EA is an effective adjuvant option for sorafenib therapy.

Key messages

● EA inhibited proliferation and induced apoptosis in HCC cells and xenograft tumors.

* Corresponding author.
** Corresponding author.
  E-mail addresses: sichongren@163.com (S. Ren), zhaoming24@126.com (M. Zhao).
[1] These authors have contributed equally to this work.

- ● EA synergistically potentiated the anticancer activity of sorafenib against HCC in both HCC cells and xenograft tumors.
- ● Combined treatment with EA and sorafenib further inhibited the MAPK and Akt/mTOR signaling pathways compared with either EA or sorafenib alone.

1. Introduction

Hepatocellular carcinoma (HCC) is the predominate form of primary liver cancer, accounting for 85–90 % of total hepatic cancers [1]. HCC leads to nearly 1 million deaths annually and is the second leading cause of cancer-related death worldwide [2]. Multimodal treatment strategies, including surgical resection, chemotherapy, radiotherapy, transarterial chemoembolization, radiofrequency ablation, immunotherapy and molecular targeted medications, are used for HCC therapy [3].

Sorafenib, an oral multikinase inhibitor, is the first targeted drug approved for patients with advanced HCC by the U.S. Food and Drug Administration. Currently, sorafenib is recognized as the standard first-line therapy for patients with advanced HCC [4]. However, only 30 % of patients with HCC respond to sorafenib, and drug resistance inevitably develops within 6 months, limiting its long-term use [5]. Although extensive studies have been conducted to enhance the therapeutic efficacy of sorafenib, continuously poor outcomes with this drug are an unmet clinical need.

Ellagic acid (EA) is a natural polyphenolic constituent derived from the naturally occurring hydrolysis of ellagitannins. These tannins are known as antitumorigenic dietary supplements found in grapes, nuts, pomegranates, berries, and dried fruits [6]. Evidence has shown that EA exhibits antitumor activity by suppressing proliferation, inducing apoptosis, and hindering inflammation, a known drug resistance process, without toxicity to normal cells [7,8]. EA was reported to attenuate concanavalin A-induced hepatitis through the toll-like receptor 2/4 and MAPK/NF-κB signaling pathways in a mouse model [9]. Several *in vitro* studies have shown the sensitivity of human HCC cell lines to the cytotoxic effects of EA treatment and its metabolite urolithin A [10–12]. EA synergistically strengthened the inhibitory activity of doxorubicin hydrochloride and cisplatin in human HCC cells and a xenograft mouse model [13,14]. However, the underlying mechanisms of its anticancer activity in HCC are still elusive. Additionally, whether it can potentiate the response of HCC tumors to sorafenib has yet to be explored extensively.

In the present study, we aimed to study the effect of EA on HCC tumor growth and its underlying mechanisms, as well as the potential efficacy in combination with sorafenib for HCC therapy. The results of this study revealed that EA inhibited HCC tumor growth by inducing apoptosis through attenuation of the MAPK and Akt/mTOR signaling pathways. Furthermore, EA synergistically potentiated the anticancer activity of sorafenib against HCC both *in vitro* and *in vivo*, an effect that may be attributed to the further inhibition of the MAPK and Akt/mTOR signaling pathways. These results suggest that EA is an effective adjuvant option for sorafenib therapy.

2. Materials and methods

2.1. Cell culture

The human HCC cell lines Huh7 (CL-0120) and Hep3B (CL-0102) were purchased from Procell Life Science & Technology Co., Ltd (Wuhan, China). Huh7 and Hep3B cells were maintained in DMEM and RPMI-1640 medium, respectively; supplemented with 10 % fetal bovine serum (XP0937, VivaCell, Shanghai, China) and 100 U/mL penicillin and 100 μg/mL streptomycin (SV30010, HyClone, UT, USA). All cell lines were cultured at 37 °C in an incubator with 5 % CO_2.

2.2. Cell viability assay

A Cell Counting Kit-8 (CCK-8) assay was used to measure cell viability. Briefly, both Huh7 and Hep3B cells were seeded in 96-well plates at 4000 cells per well for 24 h. The cells were then treated with serial concentrations of EA (HY–B0183, MedChemExpress, Monmouth Junction, NJ, USA), sorafenib (S7397, Selleck Chemicals, Houston, TX, USA) or left untreated as a control. After 96 h, both treated and untreated cells were incubated with CCK-8 (C0043, Beyotime Biotechnology, Beijing, China) for 2 h, followed by absorbance measurements at 450 nm on a spectrophotometer. The maximum concentration was 80 μM for EA and 20 μM for sorafenib and was serially diluted twofold. A log (concentration)-survival plot was used to visualize the cell growth inhibition rate. This experiment was repeated in triplicate.

2.3. 5-Ethynyl-2' -deoxyuridine (EdU) incorporation assay

EdU incorporation assay was performed according to the manufacturer's instructions (BeyoClick™ EdU Detection Kit; C0075S, Beyotime Biotechnology). All reagents used in the assay were provided by the manufacturer. Both Huh7 and Hep3B cells were seeded on coverslips in 24-well plates at 4×10^4 cells per well and treated with EA or untreated control. After 24 h, both treated and untreated cells were incubated with EdU (20 μM) for 1 h. Next, cells were washed with phosphate-buffered saline (PBS) three times and fixed with fixation buffer for 15 min at room temperature, followed by penetration for 15 min at room temperature. Cells received an additional three rounds of PBS washes followed by incubation with click reaction buffer for 30 min at 37 °C and washed again with PBS. Nuclei were stained with Hoechst at 1:1000 for 10 min at room temperature and then washed with PBS. Finally, cell-seeded and

stained coverslips were mounted and imaged using a Leica fluorescence microscope. Three random fields per slice were imaged to quantify the EdU incorporation rate, which was represented by the ratio of EdU-positive cell number to Hoechst-positive cell number. This experiment was repeated in triplicate.

2.4. Colony formation assay

Both Huh7 and Hep3B cells were seeded in 6-well plates at 1000 cells per well and incubated with EA at 10 or 20 μM or left untreated as control. Cells were fed with fresh medium and drug every 3 d over the course of 2 weeks. After the 14 d treatment, both treated and untreated cells were fixed with 4 % paraformaldehyde followed by staining with 0.1 % crystal violet (C0121, Beyotime Biotechnology) for at least 10 min. After extensive washes with water, the colonies were imaged, and colony formation efficiency was calculated by ImageJ. This experiment was repeated in triplicate.

2.5. Apoptosis analysis

Cell apoptosis analysis was performed as described previously [15]. Both Huh7 and Hep3B cells were treated with EA at 10 or 20 μM or left untreated for control for 96 h. Treated and untreated cells were trypsinized, washed with PBS, and resuspended with staining buffer containing Annexin V-APC and PI (P-CA-207, Procell, Wuhan, China) stains at room temperature for 20 min. After staining, cells were washed with PBS thrice, resuspended with PBS and subjected to flow cytometry (Novocyte, Agilent, Santa Clara, CA, USA). This experiment was repeated in triplicate.
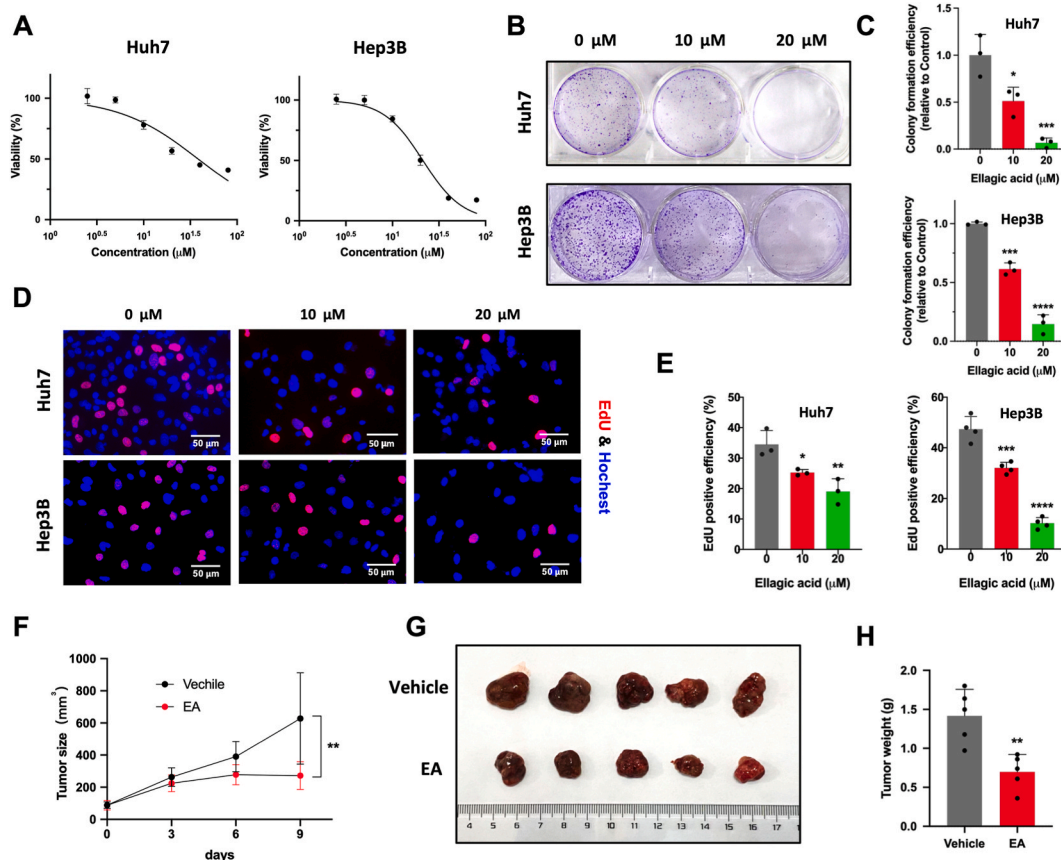
Fig. 1. EA reduces HCC growth both *in vitro* and *in vivo*. (A) Representative drug response curves of Huh7 and Hep3B cells to EA treatment. (B) EA suppresses colony formation by Huh7 and Hep3B cells. (C) Quantification of the colony formation efficiency with EA treatment. (D) EdU incorporation assay shows reduced DNA replication with EA treatment. (E) Quantification of the EdU incorporation rate in (D). (F) Growth curves of subcutaneous tumors in nude mice administered EA or vehicle. (G) Graph of tumors 9 d after EA or vehicle administration. (H) Quantification of tumor weight in (G). Results are expressed as the means ± SDs. *P* values were determined by one-way ANOVA with multiple comparison test in (C, E); two-way ANOVA with multiple comparison test in (F); unpaired two-tailed *t*-test in (H). *$P < 0.05$, **$P < 0.01$, ***$P < 0.001$, ****$P < 0.0001$.

2.6. Double staining of TUNEL and AFP

Tumor apoptosis was assessed using a TUNEL apoptosis detection kit (40306ES50, Yeasen, Shanghai, China). Paraffin sections were dewaxed with xylene, and sequentially rinsed with serial concentrations of ethanol (100, 90, 75, 50 %) and PBS for 5 min. Sections
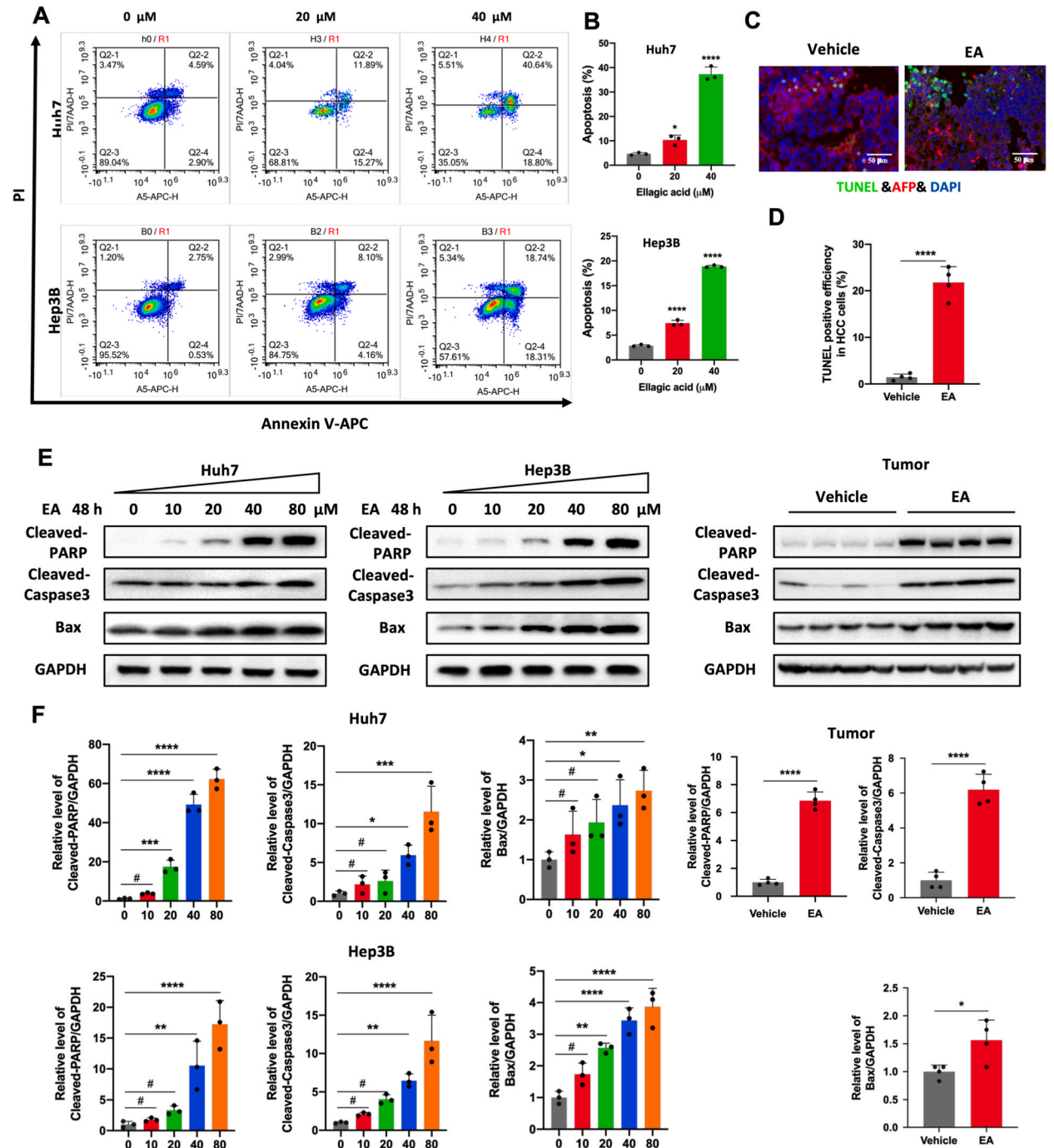
Fig. 2. EA induces apoptosis in HCC cells both *in vitro* and *in vivo*. (A) Representative images showing increased apoptosis rates in Huh7 and Hep3B cells after 4 days of EA treatment. (B) Quantification of the apoptosis rates in (A). (C) Double staining of TUNEL and AFP showing an increased apoptosis rate in HCC cells in the EA-treated xenograft mouse model. (D) Quantification of TUNEL positivity in (C). (E) Western blot analysis showing increased levels of the apoptotic proteins C-PARP, C-Caspase3 and Bax in both EA-treated cells and the xenograft mouse model. Results are expressed as the means ± SDs. (F) Quantification of protein expression level in (E). *P* values were determined by one-way ANOVA with multiple comparison test in (B, F); unpaired two-tailed *t*-test in (D). *$P < 0.05$, **$P < 0.01$, ****$P < 0.0001$.

were then incubated with goat serum (C0265, Beyotime Biotechnology) for 30 min at room temperature followed by alpha fetoprotein (AFP, 1:100, AF6159, Beyotime Biotechnology) at 4 °C overnight. Sections were washed thrice with PBS and incubated with Cy3-labeled secondary antibody (1:500, A0516, Beyotime Biotechnology). After washing with PBS thrice, sections were incubated with proteinase K (20 μg/mL in 100 μL PBS) at room temperature for 20 min. Then, additional washes with PBS were followed by incubation with 100 μL 1 × Equilibration Buffer at room temperature for 20 min. Next, sections were incubated with 50 μL TdT at 37 °C for 60 min and diamidino-phenyl-indole (DAPI, 2 μg/mL) at room temperature for 5 min, followed by mounting on microscope slides and imaging using a Leica fluorescence microscope. Three random fields per slice were imaged to quantify the rate of TUNEL positivity, represented by the TUNEL-positive cell number per area. This experiment was repeated in triplicate.

2.7. Western blot

Proteins were extracted from treated and untreated cells and xenograft tumors using RIPA lysis buffer (P0013C, Beyotime Biotechnology) supplemented with proteinase inhibitor and phosphatase inhibitor (Beyotime Biotechnology). Protein lysates were loaded into wells of a 10 or 12 % SDS−PAGE gel and separated using electrophoresis. Separated proteins were then transferred to a PVDF membrane (Millipore, Billerica, MA, USA) prior to incubation with the following antibodies overnight at 4 °C: Cleaved-caspase 3 (1:1000, 14220T, cell signaling technology [CST]), Bax (1:1000, 2772T, cell signaling technology [CST]), GAPDH (1:1000, AF7021, Affinity), *p*-ERK (1:1000, 4370T, CST), ERK (1:1000, 4695T, CST), p-P38 (1:1000, 4691T, CST), P38 (1:1000, 8690T, CST), *p*-JNK (1:1000, 4668T, CST), JNK (1:1000, 9252T, CST), *p*-Akt^{Ser473} (1:1000, 4060T, CST), *p*-Akt^{Thr308} (1:1000, 13038T, CST), Akt (1:1000, 4691T, CST), *p*-mTOR (1:500, 381548, Zen-Bioscience), mTOR (1:500, R380411, Zen-Bioscience), and cleaved-PARP (1:500, 380374, Zen-Bioscience). A Chemiluminescent HRP substrate (WBKLS0500, Millipore) was used to detect ChemiDoc XRS+ (Bio-Rad) signals. To quantify protein levels, the density of the protein bands was measured by ImageJ. The relative protein levels were normalized to GAPDH, as a loading control. This experiment was repeated in triplicate.

2.8. Xenograft assay

Animal experiments were approved by the Animal Welfare Ethics Committee at Chengdu Medical College (2023-021). Six-week-old nude mice (BALB/c-nu, female, 20–23 g) were purchased from GemPharmatech Co., Ltd, Nanjing, China, and raised in a specific pathogen–free environment in the Animal Center of Chengdu Medical College. Huh7 cells (3×10^6 cells in 100 μl PBS) were implanted into the flank of each mouse. After tumors had established and grown to a diameter of at least 0.5 cm, as shown in Fig. 1, xenografted mice were randomly divided into two groups (six mice in each group) and administered EA (60 mg/kg) or vehicle by intragastric administration. An additional experiment, as shown in Fig. 5, randomly divided xenografted mice into four groups (six mice in each group) and administered EA at 30 mg/kg, sorafenib at 10 mg/kg, both EA and sorafenib, or vehicle by intragastric administration. In both experiments, tumor length and width was monitored using a vernier caliper every 3 d for 9 d after drug administration. Tumor volume was calculated with the equation: tumor volume (mm^3) $= 0.5 \times$ length $\times$ width^2.

2.9. Statistics

GraphPad Prism 8 was used for statistical analysis. Standard statistical test including a paired or unpaired two-tailed *t*-test, one way analysis of variance (ANOVA) and two-way ANOVA were used for the analysis. All values are expressed as the means ± standard deviation. $P < 0.05$ indicated statistical significance.

3. Results

3.1. EA inhibits HCC growth both in vitro and in vivo

To elucidate the effect of EA on HCC proliferation, Huh7 and Hep3B cells were treated with serial concentrations of EA for 4 d. The CCK-8 assay showed that EA reduced cell viability in both cell lines (Fig. 1A). Additionally, EA treatment suppressed colony formation (Fig. 1B and C). EA also reduced DNA replication in Huh7 and Hep3B cells, detected by EdU incorporation assay, which is consistent with decreased cell proliferation (Fig. 1D and E). To further evaluate whether EA suppresses tumor growth *in vivo*, xenografted mice were treated with EA or vehicle by intragastric administration. Compared with that in the vehicle group, tumor growth was reduced in the EA group (Fig. 1F). Nine days after EA administration, smaller tumor sizes and lower tumor weights were observed in the EA group compared to vehicle tumors (Fig. 1G and H). These results demonstrate that EA suppresses tumor growth both *in vitro* and *in vivo*.

3.2. EA induces apoptosis both in vitro and in vivo

To elucidate whether EA induces apoptosis in HCC cells, Huh7 and Hep3B cells were treated with EA for 4 d, stained with Annexin V/PI and analyzed by flow cytometry. The results showed that EA induced apoptosis in both Huh7 and Hep3B cells (Fig. 2A and B). To determine whether EA induces apoptosis in HCC cells of xenograft mouse models, Huh7 cells were implanted into nude mice and treated with EA or vehicle control after tumor establishment. Consistent with the *in vitro* results, the TUNEL assay also indicated increased apoptosis in EA-treated xenograft mice compared to untreated vehicle xenograft mice (Fig. 2C and D). We further analyzed the levels of the apoptotic proteins, c-PARP, c-caspase 3, and Bax, which were increased in both EA-treated cells and EA-treated tumors
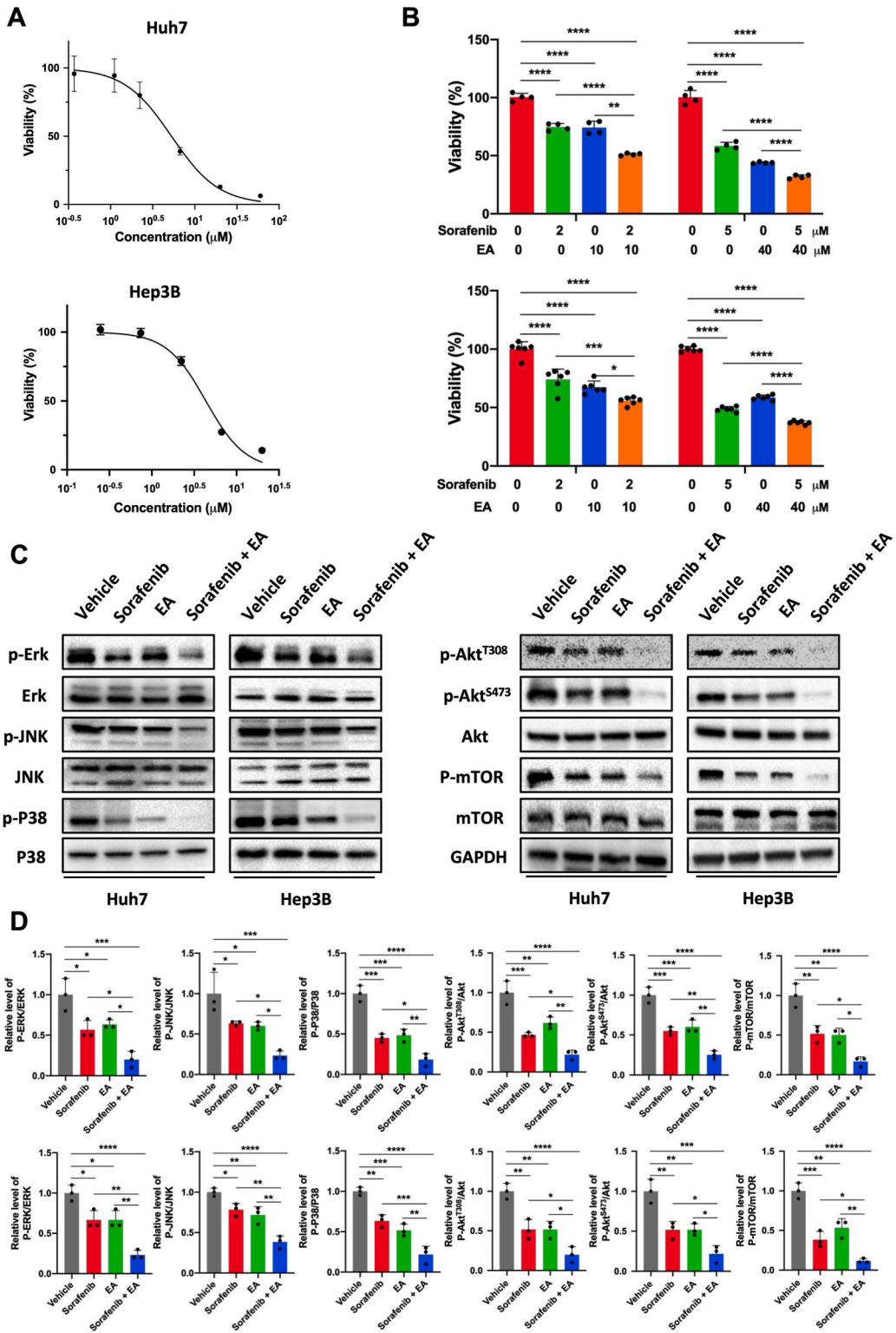
from xenograft mouse models (Fig. 2E and F). These results demonstrate that EA induces apoptosis in both *in vitro* and *in vivo* HCC models.

3.3. EA attenuates the MAPK and Akt/mTOR signaling pathways

To investigate the mechanisms by which EA mediates HCC growth arrest, transcriptome analysis was performed to study altered signaling pathways in Huh7 cells after EA incubation for 2 d. The differentially expressed genes are presented in a heatmap and a volcano plot (Fig. 3A and B). KEGG analysis was used to identify alterations in the MAPK and mTOR signaling pathways, which are
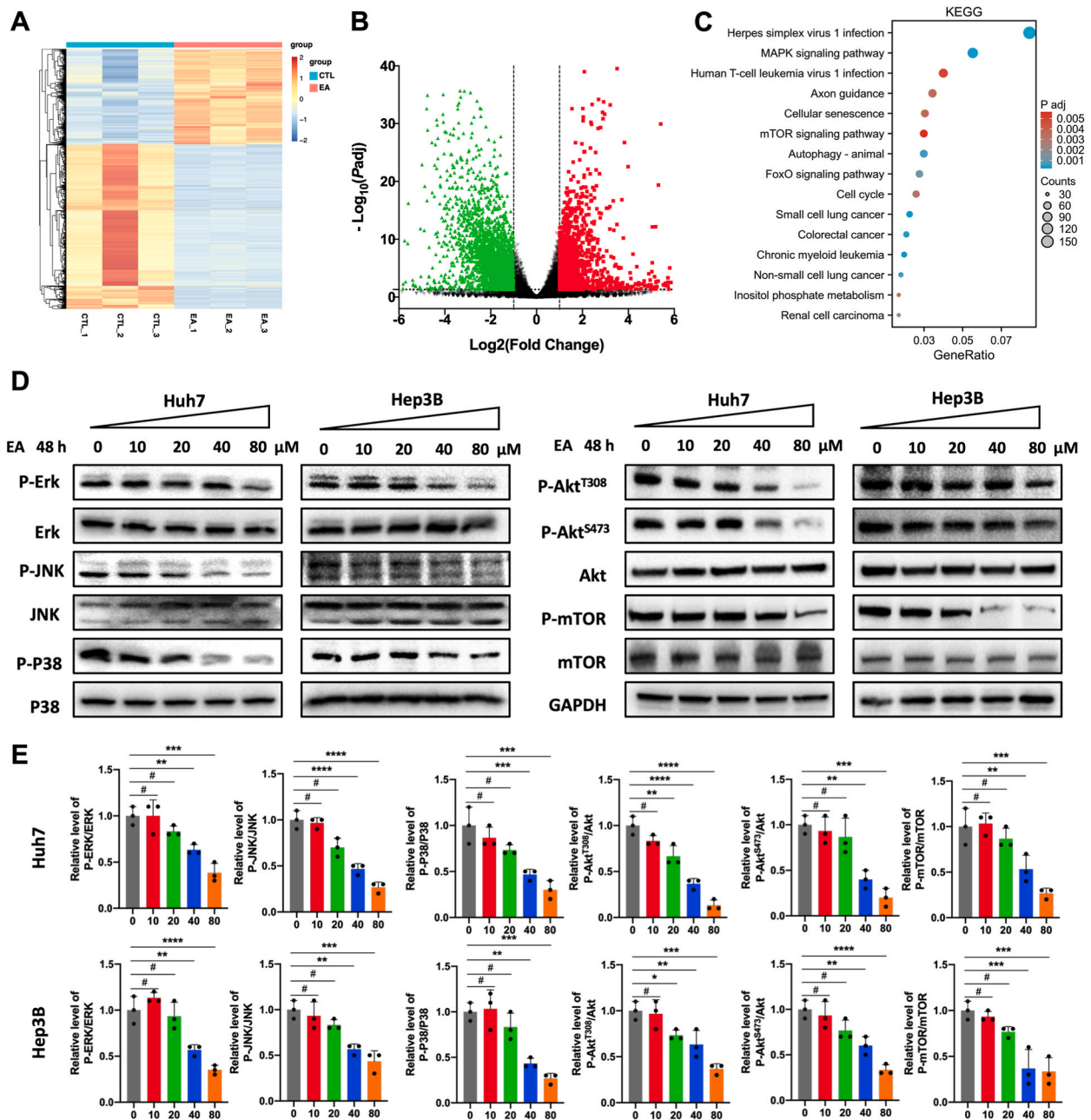

Fig. 3. EA inhibits the MAPK and Akt/mTOR signaling pathways in HCC cells. (A) Heatmap showing the differentially expressed genes in Huh7 cells treated with EA for 4 days. (B) Volcano plot showing upregulated and downregulated genes. (C) KEGG analysis results showing the enriched signaling pathways. (D) Western blot analysis showing inhibition of the MAPK and Akt/mTOR signaling pathways. (E) Quantification of protein expression level in (D). P values were determined by one-way ANOVA with multiple comparison test in (E). Results are expressed as the means ± SDs.

A Huh7 / Hep3B viability dose-response curves; **B** Viability bar graphs; **C** Western blots; **D** Relative protein level bar graphs

(caption on next page)

Fig. 4. EA potentiates the response of HCC cells to sorafenib. (A) Representative drug response curves of Huh7 and Hep3B cells to sorafenib. (B) EA and sorafenib show synergistic effects on inhibiting HCC cell growth at 4 days. IC_{75} and IC_{50} of EA are 2 and 5 μM in both cell lines; IC_{75} and IC_{50} of sorafenib is 10 and 40 μM in both cell lines. (C) Western blot analysis showing synergistic inhibition of the MAPK and Akt/mTOR signaling pathways. Cells were incubated with sorafenib (5 μM), EA (20 μM) or both for 48 h. (E) Quantification of protein expression level in (D). Results are expressed as the means ± SDs. *P* values were determined by one-way ANOVA with multiple comparison test in (B, E). *$P < 0.05$, **$P < 0.01$, ***$P <$ 0.001, ****$P < 0.0001$.
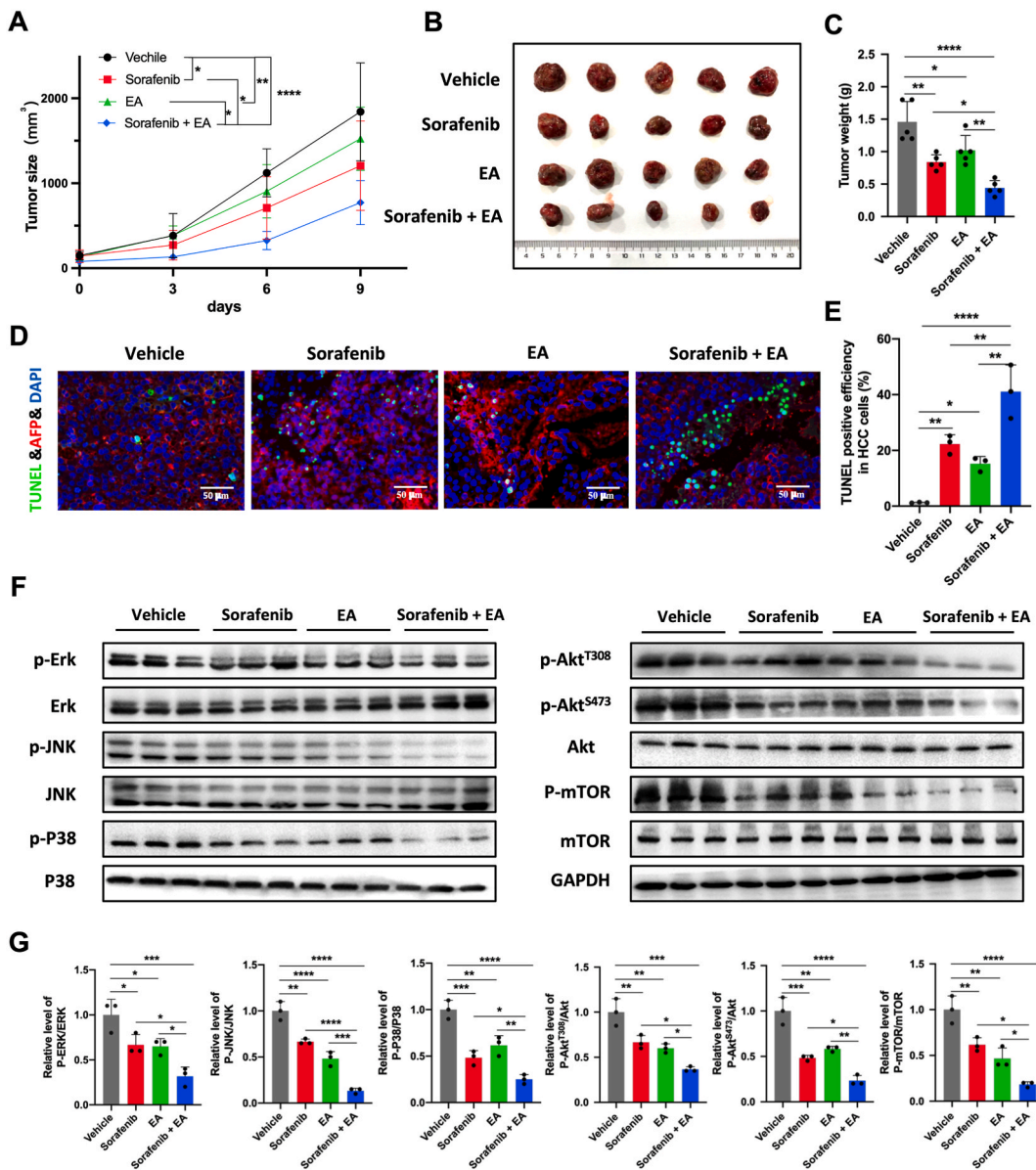
Fig. 5. EA potentiates the response of HCC to sorafenib in a xenograft mouse model. (A) Growth curves of subcutaneous tumors in nude mice administered EA, sorafenib, EA combined with sorafenib, or vehicle. (B) Graph of tumor weights 9 days after administration of EA, sorafenib, EA combined with sorafenib or vehicle. (C) Double staining of TUNEL and AFP showing an increased apoptosis rate in HCC cells in xenograft tumors from mice administered the combination of EA and sorafenib, which is quantified in (D). (E) Western blot analysis showing synergistic inhibition of the MAPK and Akt/mTOR signaling pathways in xenograft tumors. (F) Quantification of protein expression level in (E). Results are expressed as the means ± SDs. *P* values were determined by two-way ANOVA with multiple comparison test in (A); one-way ANOVA with multiple comparison test in (C, E, F). *$P < 0.05$, **$P < 0.01$, ***$P < 0.001$, ****$P < 0.0001$.

crucial for cell growth and apoptosis (Fig. 3C). Additionally, we treated both Huh7 and Hep3B cells with serial concentrations of EA for 2 d and confirmed the reduced phosphorylation of ERK, JNK, and P38 as well as Akt and mTOR with western blots, suggesting suppression of the MAPK and Akt/mTOR signaling pathways (Fig. 3D and E).

3.4. EA potentiates the response of HCC to sorafenib in vitro

Sorafenib, a classical first-line drug for patients with advanced HCC, is a multikinase inhibitor that targets both the MAPK and Akt/mTOR signaling pathways. To investigate whether the combination of EA and sorafenib could be a beneficial therapeutic strategy than sorafenib alone for HCC, we compared the cell viability targeting efficiency of EA, sorafenib, EA combined with sorafenib and vehicle control. We first determined the IC_{50} and IC_{75} of sorafenib in both Huh7 ($IC_{50} = 5$ µM, $IC_{75} = 2$ µM) and Hep3B cells ($IC_{50} = 4.3$ µM, $IC_{75} = 2.4$ µM) (Fig. 4A). The combination of EA and sorafenib at either the IC_{50} or IC_{75} showed a significantly enhanced reduction of cell viability in both Huh7 and Hep3B cells (Fig. 4B). We further observed the synergistic suppression of the MAPK and Akt/mTOR signaling pathways by the combination of EA and sorafenib (Fig. 4C and D). These results indicated that the enhanced effect of EA and sorafenib on HCC involves the inhibition of the MAPK and Akt/mTOR signaling pathways *in vitro*.

3.5. EA potentiates the response of HCC to sorafenib in vivo

To confirm whether the combination of EA with sorafenib enhances the therapeutic efficacy of sorafenib against HCC tumors, we inoculated Huh7 cells into the dorsal surface of nude mice. Xenografted mice were randomly divided into four groups, then treated with EA, sorafenib, EA combined with sorafenib or vehicle by intragastric administration. Compared to vehicle control, the tumor growth rate was decreased in both the EA group and sorafenib group and further decreased in the combination group (Fig. 5A). Additionally, while both EA and sorafenib alone reduced tumor growth, their combination showed a much higher growth reduction efficacy (Fig. 5B and C). Consistent with the apoptosis induction *in vitro*, the TUNEL assay indicated increased apoptosis in both the EA and sorafenib alone groups and a much higher apoptosis rate in the combination group (Fig. 5D and E). Additionally, proteins isolated from tumors were subjected to Western blot to confirm that phosphorylation of ERK, JNK, and P38 was reduced, as well as Akt and mTOR. This suggests that the combination of EA and sorafenib reduced activation of the MAPK and Akt/mTOR signaling pathways in the tumors (Fig. 5F and G). Taken together, these results demonstrate that EA potentiated the response of HCC to sorafenib *in vivo*.

4. Discussion

The liver is the major target organ for agent-induced toxicity. Although most drugs exhibit cytotoxicity against tumor cells in the liver, they also cause damage to normal liver cells. Therefore, an agent with anticancer activity that does not harm normal cells is an ideal candidate for cancer therapy. Phytochemicals are a potential source of anticancer agents due to low toxicities in normal tissue and minor side effects. The natural polyphenolic compound EA has been found to attenuate liver toxicity induced by cisplatin, alcohol, and carbon tetrachloride through multiple mechanisms, such as scavenging of free radicals, modulation of CYP450 enzyme activity and chelation of divalent ions [16].

Ellagitannins are antitumorigenic dietary supplements that are naturally hydrolyzed to EA and further metabolized to urolithins by intestinal flora. Then, the converted urolithins are readily absorbed by intestinal epithelial cells and transported through blood circulation [17]. Urolithins are a group of metabolites with various phenolic hydroxylation patterns and have been found to show anticancer activity in various types of tumors [18–20]. Urolithin A is a colonic metabolite of EA and was demonstrated to reduce oxidative stress and inhibit the proliferation of the HCC cell line HepG2 [12]. In the present study, the response to EA in the *in vitro* cell model is attributed to EA itself rather than the converted metabolites. However, the reduced tumor growth in the mouse model is expected to be caused by both EA and its converted metabolites.

The MAPK and Akt/mTOR signaling pathways are well understood, they inhibit apoptosis and maintain the survival of tumor cells [21,22]. These oncogenic pathways are frequently overactivated in HCC tumors [23]. As a multikinase inhibitor, sorafenib was shown to inhibit the activation of both pathways, characterized by reduced phosphorylation of ERK1/2, JNK, P38/MAPK, Akt and mTOR. Activation of the MAPK and Akt/mTOR signaling pathways in HCC cells confers resistance to sorafenib [24]. Like sorafenib, EA has been demonstrated to inhibit the MAPK and Akt/mTOR signaling pathways in this study. Furthermore, we found that the combination of EA and sorafenib further reduced the activity of these pathways. Therefore, we hypothesized that the combination of EA and sorafenib may show better therapeutic efficacy than sorafenib alone, and this hypothesis was confirmed both *in vitro* and *in vivo* in our results.

EA was reported to reduce the expression of PD-L1 on bladder cancer cells [25] and block the PD-1/PD-L1 interaction in an MC38 cell-derived colorectal cancer mouse model [26], implying that EA could attenuate immune evasion by reducing PD1/PD-L1 axis signaling to suppress tumor progression. Our previous studies showed that *anti*-PD1 antibody treatment potentiates sorafenib sensitivity in a primary cholangiocarcinoma mouse model [27]. Therefore, we hypothesized that in addition to attenuation of the MAPK and Akt/mTOR signaling pathways, the enhanced efficiency of EA combined with sorafenib might be attributed to the EA-induced reduction in PD1/PD-L1 axis signaling in an immunocompetent mouse model, a possibility that is worthy of further investigation.

5. Conclusion

In this study, we demonstrated that EA reduced HCC tumor growth by inducing apoptosis through attenuation of the MAPK and

Akt/mTOR signaling pathways. EA and sorafenib synergistically suppressed HCC growth both *in vitro* and *in vivo*. Mechanistically, combined treatment with EA and sorafenib further suppressed the MAPK and Akt/mTOR signaling pathways compared with either EA or sorafenib alone.

Funding

Data availability statement

On reasonable request to the corresponding author.

CRediT authorship contribution statement

Zhenju Tan: Methodology, Investigation. **Xuemei Li:** Validation, Methodology. **Xia Chen:** Methodology, Data curation. **Li Wang:** Data curation. **Baijun Chen:** Formal analysis. **Sichong Ren:** Writing – review & editing, Conceptualization. **Ming Zhao:** Writing – review & editing, Writing – original draft, Supervision, Funding acquisition, Conceptualization.

Declaration of competing interest

The authors declare that they have no known competing financial interests or personal relationships that could have appeared to influence the work reported in this paper.

Acknowledgments

Appendix A. Supplementary data

Supplementary data to this article can be found online at https://doi.org/10.1016/j.heliyon.2023.e23931.

References

[1] W. Yang, et al., Association of intake of whole grains and dietary fiber with risk of hepatocellular carcinoma in US adults, JAMA Oncol. 5 (6) (2019) 879–886.
[2] H. Sung, et al., Global cancer statistics 2020: GLOBOCAN estimates of incidence and mortality worldwide for 36 cancers in 185 countries, CA Cancer J Clin 71 (3) (2021) 209–249.
[3] J.M. Llovet, et al., Hepatocellular carcinoma, Nat Rev Dis Primers 7 (1) (2021) 6.
[4] R. Pinyol, et al., Molecular predictors of prevention of recurrence in HCC with sorafenib as adjuvant treatment and prognostic factors in the phase 3 STORM trial, Gut 68 (6) (2019) 1065–1075.
[5] R. Ford, et al., Lessons learned from independent central review, Eur. J. Cancer 45 (2) (2009) 268–274.
[6] J. Chen, H. Yang, Z. Sheng, Ellagic acid activated PPAR signaling pathway to protect ileums against Castor oil-induced diarrhea in mice: application of transcriptome analysis in drug screening, Front. Pharmacol. 10 (2019) 1681.
[7] V. Aishwarya, S. Solaipriya, V. Sivaramakrishnan, Role of ellagic acid for the prevention and treatment of liver diseases, Phytother Res. 35 (6) (2021) 2925–2944.
[8] J. Zhao, et al., Multiple effects of ellagic acid on human colorectal carcinoma cells identified by gene expression profile analysis, Int. J. Oncol. 50 (2) (2017) 613–621.
[9] J.H. Lee, et al., Protective effect of ellagic acid on concanavalin A-induced hepatitis via toll-like receptor and mitogen-activated protein kinase/nuclear factor κB signaling pathways, J. Agric. Food Chem. 62 (41) (2014) 10110–10117.
[10] H.M.I. Abdallah, et al., 1,8 Cineole and Ellagic acid inhibit hepatocarcinogenesis via upregulation of MiR-122 and suppression of TGF-β1, FSCN1, Vimentin, VEGF, and MMP-9, PLoS One 17 (1) (2022), e0258998.
[11] J. Li, et al., Punicalagin and ellagic acid from pomegranate peel induce apoptosis and inhibits proliferation in human HepG2 hepatoma cells through targeting mitochondria, Food Agric. Immunol. 30 (1) (2019) 897–912.
[12] Y. Wang, et al., In vitro antiproliferative and antioxidant effects of urolithin A, the colonic metabolite of ellagic acid, on hepatocellular carcinomas HepG2 cells, Toxicol. Vitro 29 (5) (2015) 1107–1115.
[13] A.M. Zaazaa, et al., Ellagic acid holds promise against hepatocellular carcinoma in an experimental model: mechanisms of action, Asian Pac. J. Cancer Prev. APJCP 19 (2) (2018) 387–393.
[14] C. Zhong, et al., Ellagic acid synergistically potentiates inhibitory activities of chemotherapeutic agents to human hepatocellular carcinoma, Phytomedicine 59 (2019), 152921.
[15] S. Sun, et al., ER stress activates TAp73α to promote colon cancer cell apoptosis via the PERK-ATF4 pathway, J. Cancer 14 (11) (2023) 1946–1955.
[16] W.R. García-Niño, C. Zazueta, Ellagic acid: pharmacological activities and molecular mechanisms involved in liver protection, Pharmacol. Res. 97 (2015) 84–103.

[17] M.A. Nuñez-Sánchez, et al., Targeted metabolic profiling of pomegranate polyphenols and urolithins in plasma, urine and colon tissues from colorectal cancer patients, Mol. Nutr. Food Res. 58 (6) (2014) 1199–1211.

[18] M. Núñez-Sánchez, et al., In vivo relevant mixed urolithins and ellagic acid inhibit phenotypic and molecular colon cancer stem cell features: a new potentiality for ellagitannin metabolites against cancer, Food Chem. Toxicol. 92 (2016) 8–16.

[19] S.G. Kasimsetty, et al., Colon cancer chemopreventive activities of pomegranate ellagitannins and urolithins, J. Agric. Food Chem. 58 (4) (2010) 2180–2187.

[20] D. Heber, Multitargeted therapy of cancer by ellagitannins, Cancer Lett. 269 (2) (2008) 262–268.

[21] J.A. McCubrey, et al., Roles of the RAF/MEK/ERK and PI3K/PTEN/AKT pathways in malignant transformation and drug resistance, Adv. Enzym. Regul. 46 (2006) 249–279.

[22] P.J. Roberts, C.J. Der, Targeting the Raf-MEK-ERK mitogen-activated protein kinase cascade for the treatment of cancer, Oncogene 26 (22) (2007) 3291–3310.

[23] T. Garcia-Lezana, J.L. Lopez-Canovas, A. Villanueva, Signaling pathways in hepatocellular carcinoma, Adv. Cancer Res. 149 (2021) 63–101.

[24] M.Y. Chen, et al., Ovatodiolide and antrocin synergistically inhibit the stemness and metastatic potential of hepatocellular carcinoma via impairing ribosome biogenesis and modulating ERK/Akt-mTOR signaling axis, Phytomedicine 108 (2023), 154478.

[25] C. Ceci, et al., Ellagic acid inhibits bladder cancer invasiveness and in vivo tumor growth, Nutrients 8 (11) (2016).

[26] J.H. Kim, et al., Unripe black raspberry (rubus coreanus miquel) extract and its constitute, ellagic acid induces T cell activation and antitumor immunity by blocking PD-1/PD-L1 interaction, Foods 9 (11) (2020) 1590.

[27] M. Zhao, et al., Cullin 3 deficiency shapes tumor microenvironment and promotes cholangiocarcinoma in liver-specific Smad 4/Pten mutant mice, Int. J. Biol. Sci. 17 (15) (2021) 4176–4191.